

Extended state observer–based improved non-singular fast terminal sliding mode for mobile manipulators

Mhmed Algrnaodi¹ , Maarouf Saad¹, Mohamad Saad², Raouf Fareh³ and Yassine Kali¹

Transactions of the Institute of
Measurement and Control
1–14

© The Author(s) 2023



Article reuse guidelines:

sagepub.com/journals-permissions

DOI: 10.1177/01423312231184513

journals.sagepub.com/home/tim



Abstract

The robust non-singular fast terminal sliding mode (NFTSM) controller is adopted in this work to solve the problem of tracking trajectory of a mobile manipulator (MM) suffering from uncertainties. The NFTSM method has the capability to ensure convergence rate and to provide good tracking accuracy and robustness against external perturbations and parameter uncertainties (total disturbances). However, the NFTSM controller needs high discontinuous gain to reject the effect of strong disturbances, which results in vibrations in the steady-state and chattering in the control law. To solve these issues, an extended state observer–based NFTSM technique is proposed for n -degree of freedom (DoF) coupling MM. The proposed method is designed to approximate and compensate in real-time the uncertainties. It also ensures robustness against total disturbances, good convergence rate, and good tracking accuracy. The stability of the proposed control is also verified based on the Lyapunov theory. Experimental works are conducted on a 5-degree-of-freedom (5-DoF) MM where the results obtained demonstrate the effectiveness of the developed technique and prove the stability of the closed-loop system.

Keywords

NFTSM method, mobile manipulators, modeling uncertainty, external disturbances, ESO, composite controller

Introduction

Nowadays, robots can carry out complex tasks. Modern applications require more advanced functionalities to accomplish the desired tasks. For this reason, robotic systems have an ongoing need to improve and develop their functional systems, to prompt or adapt their reactions to unpredicted circumstances. These missions, which require robots with a significant capability for mobility, adeptness, and manipulability of the robotic system, have certain advantages in many applications. Mobile manipulators (MMs) provide enormous opportunities to achieve wide tasks which are not achieved by the fixed-base manipulators or by the mobile base alone. An MM is a robotic system composed of a serial-link robot manipulator (RM) mounted on a wheeled mobile platform (MP). Due to different dynamics, there is a combined interaction between both dynamics of MMs. The trajectory tracking control of the MM is a built-in system including the end-effector of the arm and the mobile base designed to follow their desired trajectories. In addition, to obtain better control performance, it is realistic to take into consideration the trajectory tracking problem with uncertain parameters, non-linearity, external perturbations, and coupling effects. The control scheme of the MM trajectory tracking is still a challenging control problem and has attracted considerable attention in the control field.

Many researchers have developed various methods for real-time applications in trajectory tracking control. The

modeling and compensation of dynamic interactions in effect between both subsystems of the MM have been the focus of several studies (Yamamoto and Yun, 1994; Yu and Chen, 2002). These authors considered a modular method to calculate the dynamic equations of an MM. The Lagrange–d’Alembert formulation was used to develop the non-holonomic equations of motion of an MM in Chung and Velinsky (1998). The tracking control problem utilizing the overall dynamic model was considered in Walsh et al. (1994), including the redundancy between the RM and the MP.

In recent years, several tracking control approaches have been devoted to tackle the problem of the trajectory tracking for MMs, such as input–output linearization (Chung and Velinsky, 1998), adaptive fuzzy combined with backstepping (Zhong et al., 2013), adaptive sliding mode (SM) backstepping (Dong, 2002), adaptive control (Andaluz et al., 2012), robust

¹Electrical Engineering Department, École de Technologie Supérieure, Université du Québec, Canada

²School of Engineering, Université du Québec en Abitibi-Témiscamingue, Canada

³Electrical Engineering Department, University of Sharjah, UAE

Corresponding author:

Mhmed Algrnaodi, Electrical Engineering Department, École de Technologie Supérieure, Université du Québec, Montreal, QC H3C 1K3, Canada.

Email: mhmed.algrnaodi.1@ens.etsmtl.ca

adaptive control (Li et al., 2008; Peng et al., 2014), robust impedance control (Souzanchi et al., 2017), and recurrent neural network (RNN) (Khan et al., 2020). Moreover, decentralized controllers have been developed and applied to MMs (Fareh et al., 2017; Savino et al., 2020). However, these techniques heavily depend on the accuracies of the dynamic model and cannot guarantee good performance if the model is not well known. To achieve an excellent performance in trajectory tracking applications, the controller needs complete information on the robot dynamics. In practice, this is a challenging task and the obtained model may be considered with uncertainties, disturbances, and non-linearities. Thus, an accurate, effective, and robust method for MMs' posture control should be developed with urgent attention.

SM control has gained tremendous popularity for its remarkable features such as strong insensitivity to a wide range of perturbations and uncertainties, fast transient response, and simplicity (Gu and Wang, 2018, 2019; Yang et al., 2013). Sliding mode control (SMC) is based on a reliable and systematic approach to achieving robust control, ensuring system stability and consistent performance, even in the presence of modeling uncertainties and disturbances. Moreover, SMC allows for a design tradeoff between tracking performance and smoothing control discontinuity, making it practical for implementation in most applications (Yang et al., 2012). There are two typical SMC methods: linear SMC and non-linear SMC. Linear SMC is asymptotically stable, while non-linear SMC may result in finite convergence (Wang et al., 2017; Yang et al., 2012). However, the conventional SM with linear sliding manifold cannot ensure finite-time convergence of the system state to the equilibrium point (Jin et al., 2009). To ensure this latter, a terminal sliding mode (TSM) (Khawwaf et al., 2017; Mobayen and Javadi, 2017) that uses non-linear sliding manifold was introduced. The TSM, however, has a singularity problem since terms with negative fractional powers may exist (Wu et al., 1998). Non-singular terminal sliding mode (NTSM) was proposed and used to address the problem of singularity (Chen and Lin, 2010). NTSM has good accuracy of tracking, fast convergence, and the property of avoidance of singularity (Madani et al., 2016a, 2016b) and continuous non-singular terminal SMC (Rauf et al., 2022). Moreover, a new non-singular fast terminal sliding mode (NFTSM) controller for non-linear dynamic systems is proposed in Yang and Yang (2011). It is designed based on SM theory while overcoming the singularity problem and ensuring the system's convergence in finite time (Boukattaya et al., 2018; Feng et al., 2002; Yang and Yang, 2011).

As compared to the developed SM surfaces, the NFTSM avoids singularities and has a fast finite-time reaching even when the state is far from the equilibrium point (Boukattaya et al., 2018). In view of these promising features, the NFTSM controller has gained popularity for high-accurate tracking control problems in robotic systems such as in RM (Boukattaya et al., 2018; Geng et al., 2014; Lu et al., 2022), robotic knee prosthesis (Huang et al., 2022), underactuated quadrotor UAV (Labbadi and Cherkaoui, 2020), and mobile lower limb exoskeleton (Hernandez et al., 2020). Furthermore, non-singular fast terminal sliding mode control

(NFTSMC) techniques have been a few works published recently to solve the problem of tracking trajectory of MM.

In MMs, there is a strong coupling between MP and RM subsystems. It is more meaningful to consider disturbance rejection problem in a complete MM system. However, most of the controllers mentioned above require complete information on the robot dynamics to achieve high performance in trajectory tracking applications.

Because of the uncertainties and complexity, obtaining the upper bound in real-time applications may be difficult. As a result, the SM design introduced the problem associated with the bounded value of unknown uncertainty and dynamic perturbations. Several studies, such as observers-based controllers (Xu et al., 2019), adaptive methods (Boukattaya et al., 2018), and neural networks (Taghavifar and Rakheja, 2019), have been presented to overcome this dependence.

This paper presents an extended state observer (ESO)-based NFTSM scheme for an MM system subject to unmodeled dynamics and disturbances to address the above-mentioned challenging problems. The ESO is used to approximate the system disturbance, improving the control system's robustness and efficiency (Gao et al., 2001; Han, 2009). The ESO does not depend on a complete system model information, including external perturbations and dynamic uncertainties, estimated along with the original state variables. Therefore, the used observer is an important part of the active disturbance rejection control (ADRC) technique (Song et al., 2018; Xing et al., 2011; Zhang et al., 2020; Zhao et al., 2018).

It is worth noting that all the attitude control approaches used the ESO approximation for the total disturbances of the system based on non-linear SM (Zhang et al., 2020), NTSM (Sun and Liu, 2020; Wu et al., 2019), and continuous fast terminal sliding mode (CFTSM) (Xu et al., 2019; Wang et al., 2017), but neither of them has considered NFTSM. To the best of our knowledge, there are little works that designed and implemented the NFTSM for MM systems in real-time, which motivates us to carry out the current work.

In this paper, a technique ESO-based NFTSM is proposed as a composite solution for achieving good trajectory tracking in an MM system subject to external disturbances and parameter uncertainties. To accomplish this, an ESO is used to estimate the total system disturbances, which is then utilized for feed-forward compensation. Unlike previous research, this technique has been successfully applied in real-time for an MM system, resulting in improved suppression of continuous disturbances even under complex non-linear dynamics. The observer-based controller employed in this approach integrates the benefits of ESO, NFTSM, and robust terms to produce significantly improved experimental outcomes in terms of trajectory tracking, despite the presence of unknown system uncertainties. The main contributions of this paper are given as follows. (1) This paper provides a composite NFTSM technique with ESO (ESO-based NFTSM) to ensure a good trajectory tracking for an MM system. The ESO can estimate the system total disturbances to be used later as feed-forward compensation. (2) Compared with the previous research works, real-time application of the ESO-based NFTSM controller is done for an MM that greatly improves MM's ability to suppress continuous disturbances under a complex non-

linear dynamic model. (3) The proposed observer-based controller inherits the benefits of ESO, NFTSM, and the robust term, resulting in significantly improved trajectory tracking experimental results despite the existence of the unknown system uncertainty.

The rest of this paper is organized as follows. Section “Preliminaries and notation” presented the preliminaries and the notation used throughout this paper. A brief description of the kinematic model and deriving the dynamic model of the MM system, and the control objective are shown in section “Description of MM and control objective.” The control design scheme of the proposed ESO-based NFTSM is presented in section “ESO-based NFTSM controller design,” along with the stability analysis of the proposed technique. Section “Experiments and discussion” illustrates the validation and effectiveness of the developed controller. Finally, the conclusion of this paper is summarized in section “Conclusion.”

Preliminaries and notation

Throughout this paper, the following notations are used.

For $x = [x_1, \dots, x_n]^T \in \mathbb{R}^n$ that is a variable vector, the fractional power of vectors is defined as

$$\begin{aligned} |x|^a &= [|x_1|^{a_1}, \dots, |x_n|^{a_n}]^T \in \mathbb{R}^n \\ |x|^a &= \text{diag}(|x_1|^{a_1}, \dots, |x_n|^{a_n}) \in \mathbb{R}^{n \times n} \end{aligned}$$

while the vector $\text{sign}^a(x) \in \mathbb{R}^n$ is defined as

$$\begin{aligned} \text{sign}^a(x) &= \text{diag}(\text{sign}(x)) \cdot |x|^a \\ &= [|x_1|^{a_1} \text{sign}(x_1), \dots, |x_n|^{a_n} \text{sign}(x_n)]^T \end{aligned}$$

where the $\text{sign}(x_i)$ for $i = 1, 2, \dots, n$ is defined as

$$\text{sign}(x_i) = \begin{cases} 1 & \text{if } x_i > 0 \\ 0 & \text{if } x_i = 0 \\ -1 & \text{if } x_i < 0 \end{cases}$$

Then, if $a_i \geq 1$ for $i = 1, \dots, n$, it follows that

$$\begin{aligned} \frac{d}{dt} \text{sign}^a(x) &= a |x|^{a-I_n} \dot{x} \\ &= [a_1 \dot{x}_1 |x_1|^{a_1-1}, \dots, a_n \dot{x}_n |x_n|^{a_n-1}]^T \end{aligned} \quad (1)$$

where $a = \text{diag}(a_1, a_2, \dots, a_n)$, and I_n is the n -dimensional unit matrix.

Description of MM and control objective

This section describes the kinematic model and derives the dynamic model of the n -DoF MM in the Cartesian space. The Lagrangian technique is considered for the MM system (Li and Ge, 2013) illustrated in Figure 1, where a three-link robotic manipulator is mounted upon the center of a wheeled MP. In the MP, the two front wheels are active, and the two rear wheels are passive. The full MM system has n -DoF,

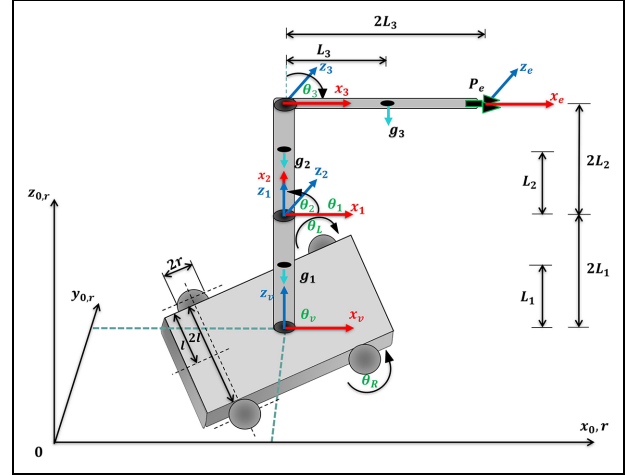


Figure 1. The system of n -DoF MM.

where the RM is subject to a holonomic constraint, and the MP is subject to a non-holonomic constraint.

Kinematics

In most robot applications, the desired trajectory is defined in the Cartesian space. P_e illustrates the position/orientation vector of the MM end-effector as shown in Figure 1. The MM can be represented by the generalized coordinates $q = [q_v^T, \theta_a^T]^T$, where $q_v = [X_v, Y_v, \phi_v]^T \in \mathbb{R}^{n_v}$ and $\theta_a = [\theta_1, \dots, \theta_{n_a}]^T \in \mathbb{R}^{n_a}$ are the state vectors of the MP and the RM, respectively, and $n = n_v + n_a$. The relationship between the generalized coordinates of the MM, its derivative $\dot{q} \in \mathbb{R}^n$, and the end-effector velocity, $V_e \in \mathbb{R}^n$, is described as follows (Brahmi et al., 2016)

$$V_e = J_e(q) \dot{q} \quad (2)$$

where $J_e(q) \in \mathbb{R}^{n \times n}$ is the Jacobian matrix and $\dot{q} = [\dot{q}_v^T, \dot{\theta}_a^T]^T$ with $\dot{q}_v = [\dot{X}_v, \dot{Y}_v, \dot{\phi}_v]^T$ is the linear/angular velocity vector of the MP, and $\dot{\theta}_a = [\dot{\theta}_1, \dots, \dot{\theta}_{n_a}]^T$ is the joint velocity vector of the RM.

Dynamic model

Using the Lagrangian technique, mathematical modeling in this paper is based on the coupled dynamics of the MP and the RM is obtained by the following equation (Li et al., 2007, 2008b)

$$M(q) \ddot{q} + C(q, \dot{q}) \dot{q} + G(q) + \tau_d = B(q) \tau - A^T(q) \lambda \quad (3)$$

where $M(q) \in \mathbb{R}^{n \times n}$, $C(q, \dot{q}) \in \mathbb{R}^n$, and $G(q) \in \mathbb{R}^n$ denote the positive-definite and symmetric inertia matrix, the centrifugal and Coriolis forces matrix, and the gravitational vector, respectively, q represents the position vector of the MM system, $\tau_d \in \mathbb{R}^n$ denotes the vector of external perturbations, $B(q) \in \mathbb{R}^{n \times k}$ represents the full-rank input transformation matrix, $\tau \in \mathbb{R}^k$ denotes the input control vector, $A(q) \in \mathbb{R}^{k \times n}$

is a constraint matrix, $\lambda \in \mathbb{R}^k$ is the constraint force vector, and are represented as

$$\begin{aligned} M(q) &= \begin{bmatrix} M_{n_v} & M_{n_v, n_a} \\ M_{n_a, n_v} & M_{n_a} \end{bmatrix}, C(q) = \begin{bmatrix} C_{n_v} & C_{n_v, n_a} \\ C_{n_a, n_v} & C_{n_a} \end{bmatrix} \\ G(q) &= \begin{bmatrix} G_{n_v} \\ G_{n_a} \end{bmatrix}, \tau_d = \begin{bmatrix} \tau_{dn_v} \\ \tau_{dn_a} \end{bmatrix}, B(q) = \begin{bmatrix} B_{n_v} & 0 \\ 0 & B_{n_a} \end{bmatrix} \\ \tau &= \begin{bmatrix} \tau_{n_v} \\ \tau_{n_a} \end{bmatrix}, A^T(q) = \begin{bmatrix} A_{n_v}^T & 0 \\ 0 & 0 \end{bmatrix}, \lambda = \begin{bmatrix} \lambda_{n_v} \\ \lambda_{n_a} \end{bmatrix} \end{aligned}$$

The MP is subjected to non-holonomic constraints. Therefore, the following equation represents the velocity constraints as given in Li et al. (2007) and (2008b)

$$A_{n_v}(q_v)\dot{q}_v = 0 \quad (4)$$

where $A_{n_v}(q_v) \in \mathbb{R}^{d \times n_v}$ is the kinematic constraint matrix, and d is the number of non-integrable constraints.

Assume $S(q_v) \in \mathbb{R}^{n_v \times (n_v - d)}$ to be the orthocomplement of $A_{n_v}(q_v)$, and (Li and Ge, 2013)

$$S^T(q_v)A_{n_v}^T(q_v) = 0 \quad (5)$$

where

$$S(q_v) = \begin{bmatrix} \cos(\phi_v) & \sin(\phi_v) & 0 \\ 0 & 0 & 1 \end{bmatrix}^T$$

and has a set of smooth and linearly independent vector fields that is obtained by spanning the null space of $A_{n_v}(q_v)$. Note that $S^T(q_v)S(q_v)$ is of full rank.

From the constraints (4) and (5), let the auxiliary vector $\dot{\eta} \in \mathbb{R}^{n_v - d}$, such that

$$\dot{q}_v = S(q_v)\dot{\eta} \quad (6)$$

which is the kinematic model of the non-holonomic MP subsystem. Differentiating equation (6) yields to

$$\ddot{q}_v = \dot{S}(q_v)\dot{\eta} + S(q_v)\ddot{\eta} \quad (7)$$

where $\dot{\eta} = [v_v, w_v]^T$ with v_v as the linear velocity and w_v as the angular velocity of the MP.

Let θ_L and θ_R be, respectively, the left and the right angular positions, and $\dot{\theta}_L$ and $\dot{\theta}_R$ be, respectively, the left and the right angular velocities of the MP, where the velocity vector of the MP is denoted as $\dot{\theta}_v = [\dot{\theta}_R, \dot{\theta}_L]^T$. Then, the kinematic model of the non-holonomic system can be expressed as follows

$$\dot{\eta} = R(q_v)\dot{\theta}_v \quad (8)$$

where

$$R(q_v) = \begin{bmatrix} \frac{r}{2} & \frac{r}{2} \\ \frac{r}{2l} & -\frac{r}{2l} \end{bmatrix}$$

Thus

$$H(q_v) = S(q_v)R(q_v) = \begin{bmatrix} \frac{r}{2} \cos(\phi_v) & \frac{r}{2} \sin(\phi_v) & \frac{r}{2l} \\ \frac{r}{2} \cos(\phi_v) & \frac{r}{2} \sin(\phi_v) & -\frac{r}{2l} \end{bmatrix}^T \quad (9)$$

where r is the wheel radius and $2l$ is the platform width as shown in Figure 1.

Considering equations (5), (6), and (7), the term of the non-holonomic constraint $A^T(q)\lambda$ can be eliminated from equation (3). Then, the dynamics in equation (3) can be reformulated as

$$\bar{M}(\theta)\ddot{\theta} + \bar{C}(\theta, \dot{\theta})\dot{\theta} + \bar{G}(\theta) = \bar{\tau} - \bar{\tau}_d \quad (10)$$

where $\theta = [\theta_v^T, \theta_a^T]^T$ are the generalized coordinates with $\theta_v = [\theta_R, \theta_L]^T$ being the angular position of the MP, $\dot{\theta} = [\dot{\theta}_R, \dot{\theta}_L, \dot{\theta}_1, \dots, \dot{\theta}_{n_a}]^T$, and

$$\begin{aligned} \bar{M}(\theta) &= \begin{bmatrix} H^T M_{n_v} H & H^T M_{n_v, n_a} \\ M_{n_a, n_v} H & M_{n_a} \end{bmatrix} \in \mathbb{R}^{\bar{n} \times \bar{n}}, = \begin{bmatrix} H^T G_{n_v} \\ G_{n_a} \end{bmatrix} \in \mathbb{R}^{\bar{n}} \\ \bar{C}(\theta, \dot{\theta}) &= \begin{bmatrix} H^T M_{n_v} \dot{H} + H^T C_{n_v} H & H^T C_{n_v, n_a} \\ M_{n_a, n_v} \dot{H} + C_{n_a, n_v} H^T & C_{n_a} \end{bmatrix} \in \mathbb{R}^{\bar{n} \times \bar{n}} \\ \bar{\tau}_d &= \begin{bmatrix} H^T \tau_{dn_v} \\ \tau_{dn_a} \end{bmatrix} \in \mathbb{R}^{\bar{n}}, \bar{\tau} = \bar{B}\tau \in \mathbb{R}^{\bar{n}}, \bar{B} = \begin{bmatrix} H^T B_{n_v} & 0 \\ 0 & B_{n_a} \end{bmatrix} \end{aligned}$$

where $\bar{n} = n_a + n_v - d$. The mathematical model in equation (10) verifies (Li et al., 2008a).

Property 1. \bar{M} is a positive-definite and symmetric matrix.

Property 2. $S = \bar{M} - 2\bar{C}$ is a skew symmetric matrix, that is, $\forall z \in \mathbb{R}^{\bar{n}}$, we have $z^T(\bar{M} - 2\bar{C})z = 0$.

Remark 1. In this paper, the MM robot is considered as a fully actuated arm mounted on the holonomic mobile platform. There is a dimension reduction of the state in equation (11) compared with equation (4) due to the kinematic constraints.

The uncertainties and the external perturbations acting on the MM system are unknown. For this reason, they should be estimated during the control design in order to avoid any undesired behavior.

Control objective

According to Properties 1 and 2, and considering that $\bar{M}(\theta) = \bar{M}_k(\theta) + \bar{M}_u(\theta)$ with $\bar{M}_k(\theta)$ and $\bar{M}_u(\theta)$ denote, respectively, the known and the unknown parts of the matrix $\bar{M}(\theta)$, a dynamic model of MM system containing the uncertain dynamic and external perturbations, which is defined in equation (10), can be rewritten as

$$\ddot{\theta} = f(\theta, \dot{\theta}) + D(\theta)\bar{\tau} \quad (11)$$

where $f(\theta, \dot{\theta}) = -D(\theta)(\bar{\tau}_d + \bar{M}_u(\theta)\ddot{\theta} + \bar{C}(\theta, \dot{\theta})\dot{\theta} + \bar{G}(\theta))$ is considered as the ‘‘total disturbance’’ of the five joints MM, including the dynamic coupling effects between the RM and the MP, the perturbations and the uncertain dynamics, and $D(\theta) = \bar{M}_k^{-1}(\theta)$.

Define $x_1 = \theta$ and $x_2 = \dot{\theta}$, respectively. The model dynamics equation (11) can be written as

$$\begin{cases} \dot{x}_1 = x_2 \\ \dot{x}_2 = f(x_1, x_2) + D(x_1)\bar{\tau} \end{cases} \quad (12)$$

Suppose that the reference signal is described by θ_d and its derivative $\dot{\theta}_d$. According to the dynamic system of MM in equation (12), the tracking error can be expressed as

$$\begin{cases} e_1 = x_1 - x_d \\ e_2 = \dot{x}_1 - \dot{x}_d = x_2 - \dot{x}_d \end{cases} \quad (13)$$

where e_1 and $e_2 \in \mathbb{R}^{\bar{n}}$ are, respectively, the measured position and the measured velocity of the tracking errors for the system, and $x_d = \theta_d$ is the known desired position trajectory generated in the workspace while \dot{x}_d represents its first time derivative.

Substituting equation (12) into the time derivative of equation (13), the error system dynamics can be written as

$$\begin{cases} \dot{e}_1 = e_2 \\ \dot{e}_2 = f(x_1, x_2) + D(x_1)\bar{\tau} - \ddot{x}_d \end{cases} \quad (14)$$

The control objective here is to construct a convenient ESO-based NFTSM for the considered non-linear system that ensures the system position vector θ follows its reference vector θ_d in the presence of external perturbations and uncertainties. The inverse kinematics is used to obtain the joint space desired trajectory θ_d from the Cartesian position/orientation trajectory P_d . The following assumption is required to achieve this goal.

Assumption 1. The total perturbations $f(x_1, x_2)$ are generally unknown. Assume that they are bounded and differentiable, such as there exists a positive constant $\mu > 0$ verifying (Van et al., 2016)

$$\|f(x_1, x_2)\| \leq \mu \quad (15)$$

with $\|f(x_1, x_2)\|$ represents the Euclidean norm of $f(x_1, x_2)$.

ESO-based NFTSM controller design

An ESO-based NFTSM scheme is proposed to handle the perturbations and the uncertainties due to its robustness. An ESO is used to estimate the total disturbances of the MM system in order to reduce the interferences of uncertainties from dynamic system. When the NFTSM and ESO are combined, the closed-loop control system becomes more effective in dealing with process disturbances and uncertainties.

NFTSM controller design

SM design typically consists of three steps: (1) the selection of the sliding manifold; (2) the design of the equivalent control part; and (3) the design of the discontinuous control part. The following NFTSM surface is introduced in the first step (Yang and Yang, 2011)

$$s = e_1 + k_1 \text{sign}^{\sigma_1}(e_1) + k_2 \text{sign}^{\sigma_2}(e_2) \quad (16)$$

where $k_1 = \text{diag}(k_{11}, \dots, k_{1\bar{n}})$, $k_2 = \text{diag}(k_{21}, \dots, k_{2\bar{n}})$, $\sigma_1 = \text{diag}(\sigma_{11}, \dots, \sigma_{1\bar{n}})$, and $\sigma_2 = \text{diag}(\sigma_{21}, \dots, \sigma_{2\bar{n}})$ with $k_{1i} > 0$, $k_{2i} > 0$, $\sigma_{1i} > \sigma_{2i}$, and $1 < \sigma_{2i} < 2$, respectively, for every $i = 1, 2, \dots, \bar{n}$. The NFTSM surface equation (16) can

ensure singularity avoidance and fast finite-time convergence for any given initial condition.

When $\dot{s} = 0$ is achieved, the system dynamics are equivalent to the non-linear differential equation shown as follows

$$e_2 + k_1 \sigma_1 [e_1]^{\sigma_1 - I_{\bar{n}}} \cdot e_2 + k_2 \sigma_2 [e_2]^{\sigma_2 - I_{\bar{n}}} \cdot \dot{e}_2 = 0 \quad (17)$$

The following is a definition of the overall control law

$$\bar{\tau} = D^{-1}(x_1)(\bar{\tau}_{eq} + \bar{\tau}_b) \quad (18)$$

$$\bar{\tau}_{eq} = -([e_2]^{\sigma_2 - I_{\bar{n}}})^{-1} \sigma_2^{-1} k_2^{-1} (I_{\bar{n}} + k_1 \sigma_1 [e_1]^{\sigma_1 - I_{\bar{n}}}) e_2 - f(x_1, x_2) + \ddot{x}_d \quad (19)$$

To satisfy the SM reaching conditions, a robust control law $\bar{\tau}_b$ is designed by taking into account the total disturbances as

$$\bar{\tau}_b = -k_3 s - k_4 \text{sign}(s) \quad (20)$$

where $k_3 = \text{diag}(k_{31}, \dots, k_{3\bar{n}})$ and $k_4 = \text{diag}(k_{41}, \dots, k_{4\bar{n}})$ are the positive-definite matrices, respectively, and satisfy $k_{3i}, k_{4i} > 0$ for $i = 1, 2, \dots, \bar{n}$.

The expression of the overall control can be obtained using the above formulas as follows

$$\bar{\tau} = D^{-1}(x_1) \left(-([e_2]^{\sigma_2 - I_{\bar{n}}})^{-1} \sigma_2^{-1} k_2^{-1} (I_{\bar{n}} + k_1 \sigma_1 [e_1]^{\sigma_1 - I_{\bar{n}}}) e_2 - f(x_1, x_2) + \ddot{x}_d - k_3 s - k_4 \text{sign}(s) \right) \quad (21)$$

Remark 2. In practice, the function $f(x_1, x_2)$ in relation (19) is unknown. Only an estimation of $f(x_1, x_2)$ can be obtained. This issue will be considered later in this paper.

Theorem 1. If the NFTSM surface for the system (12) is selected as equation (16), and $\bar{\tau}$ is designed as equation (21) to control it, then the system trajectory will converge asymptotically to zero within a finite time. Furthermore, no singularity will occur during the entire process.

Proof. The time derivative of equation (16) is calculated as

$$\dot{s} = e_2 + k_1 \sigma_1 [e_1]^{\sigma_1 - I_{\bar{n}}} \cdot e_2 + k_2 \sigma_2 [e_2]^{\sigma_2 - I_{\bar{n}}} \cdot \dot{e}_2 \quad (22)$$

Thus, substituting the expression (14) into equation (21), we have

$$\dot{s} = e_2 + k_1 \sigma_1 [e_1]^{\sigma_1 - I_{\bar{n}}} \cdot e_2 + k_2 \sigma_2 [e_2]^{\sigma_2 - I_{\bar{n}}} \cdot (f(x_1, x_2) + D(x_1)\bar{\tau} - \ddot{x}_d) \quad (23)$$

After substituting the control law (21) into equation (23), the \dot{s} becomes as follows

$$\dot{s} = -k_2 \sigma_2 [e_2]^{\sigma_2 - I_{\bar{n}}} \cdot (k_3 s + k_4 \text{sign}(s)) \quad (24)$$

For the stability analysis, the Lyapunov function $V_1 = 0.5 s^T s$ will be considered and then its derivative is computed as

$$\begin{aligned} \dot{V}_1 &= -s^T k_2 \sigma_2 [e_2]^{\sigma_2 - I_{\bar{n}}} \cdot (k_3 s + k_4 \text{sign}(s)) \\ &\leq -\eta_1 V_1 - \eta_2 V_1^{1/2} \leq 0 \end{aligned} \quad (25)$$

where $\eta_1 = \lambda_{\min}(k_2 \sigma_2 |e_2|^{\sigma_2 - k_3}) > 0$, and $\eta_2 = \lambda_{\min}(k_2 \sigma_2 |e_2|^{\sigma_2 - k_4} \sqrt{2}) > 0$. According to the Lyapunov theory, the closed-loop system dynamics is asymptotically stable (the selected sliding manifold converges to zero $s = 0$).

The above equation can be rewritten as

$$dt \leq \frac{-dV_1}{\eta_1 V_1 + \eta_2 V_1^{1/2}} = \frac{-V_1^{-1/2} dV_1}{\eta_1 V_1^{1/2} + \eta_2} = -2 \frac{dV_1^{1/2}}{\eta_1 V_1^{1/2} + \eta_2} \quad (26)$$

Assume that t_r is the required time to reach $s = 0$ (i.e. $V_1(t_r) = 0$) starting from an initial surface $s(0) \neq 0$. Then, by taking the integration of both sides of equation (26) yields

$$\int_0^{t_r} dt \leq \int_{V_1(0)}^{V_1(t_r)} -2 \frac{dV_1^{1/2}}{\eta_1 V_1^{1/2} + \eta_2} \quad (27)$$

After a simple calculation, we have

$$t_r \leq \frac{2}{\eta_1} \ln \left(\frac{\eta_1 V_1^{1/2}(0) + \eta_2}{\eta_2} \right) \quad (28)$$

According to the Lyapunov theory, the NFTSM surface s expressed in equation (16) converges to zero at a finite time t_r . Therefore, despite the existence of total disturbance, the tracking error will achieve convergence to zero in finite time if $s = 0$. This completes the proof.

ESO

Here, an ESO is developed to cope with the total disturbances of the \bar{n} -DoF MM system (12). Its merit is that it is simpler to implement and independent of the dynamic model of the plant (Gao et al., 2001). That is, the fundamental mechanism of ESO is to estimate the total disturbance via its observer (Huang and Xue, 2014). From the idea of ESO theory, the total disturbances are expanded as an extended state for the system in equation (12) which are estimated and compensated by the observer and a controller, respectively (Algrnaodi et al., 2021; Fareh et al., 2021; Zhao et al., 2019).

In the present context, by defining $x_3 = f(x_1, x_2)$ as the extra state variable of the system, x_3 is the extended state vector.

The robot dynamic system in equation (12) can be rewritten in state-space form as

$$\begin{cases} \dot{x}_1 = x_2 \\ \dot{x}_2 = x_3 + D(x_1)\bar{\tau} \\ \dot{x}_3 = h(t) \end{cases} \quad (29)$$

where $h(t)$ is the derivative of x_3 and is the unknown part required for the implementation of the control law $\bar{\tau}$. Note that $h(t)$ is bounded in practice.

Defining \hat{x}_3 as the estimation of x_3 , the simplest way to estimate x_3 is using equation (12) as

$$\hat{x}_3(t) = -(D(x_1)\bar{\tau} - \dot{x}_2) \quad (30)$$

which needs the measurement of the acceleration \dot{x}_2 . However, the acceleration is not available for measurement. For this reason, the ESO will be utilized.

The ESO proposed in Han (2009) is a non-linear observer employed to estimate x_3 . From equation (29), we construct an ESO in the form of

$$\begin{cases} \dot{e}_1 = \hat{x}_1 - x_1 \\ \dot{\hat{x}}_1 = \hat{x}_2 - \beta_1 e_1 \\ \dot{\hat{x}}_2 = \hat{x}_3 - \beta_2 f_1(e_1) + D(x_1)\bar{\tau} \\ \dot{\hat{x}}_3 = -\beta_3 f_2(e_1) \end{cases} \quad (31)$$

where $e_1 \in \mathbb{R}^{\bar{n}}$ is the observer's error for the state $x_1 \in \mathbb{R}^{\bar{n}}$; $\hat{x}_i \in \mathbb{R}^{\bar{n}}$ are the observer's output and are the estimation of state variables $x_i \in \mathbb{R}^{\bar{n}}$; $\beta_i \in \mathbb{R}^{\bar{n} \times \bar{n}}$ are the observer's gains with $i = 1, 2, 3$; $f_\chi(e_1) \in \mathbb{R}^{\bar{n}}$ for $\chi = 1, 2$ are two different non-linear functions applied to increase the convergence speed of the observer's signals with

$$f_\chi(e_1) = [fal_{\chi 1}(e_{11}, \alpha_\chi, \delta), \dots, fal_{\chi \bar{n}}(e_{1\bar{n}}, \alpha_\chi, \delta)]^T$$

and the fal functions are selected for $\chi = 1, 2$ as (Han, 2009)

$$fal_\chi(e_{1j}, \alpha_\chi, \delta) = \begin{cases} |e_{1j}|^{\alpha_\chi} \text{sign}(e_{1j}), & |e_{1j}| > \delta \\ e_{1j}/\delta^{1-\alpha_\chi}, & |e_{1j}| \leq \delta \end{cases} \quad (32)$$

In this case, $j = 1, \dots, \bar{n}$, α_1 , α_2 , and δ are the positive parameters to be determined, and

$$\begin{cases} \beta_1 = \text{diag}(3w_0, 3w_0, 3w_0, 3w_0, 3w_0) \\ \beta_2 = \text{diag}(3w_0^2, 3w_0^2, 3w_0^2, 3w_0^2, 3w_0^2) \\ \beta_3 = \text{diag}(w_0^3, w_0^3, w_0^3, w_0^3, w_0^3) \end{cases} \quad (33)$$

Here, β_i is obtained by the observer bandwidth w_0 where $w_0 = 3w_c$ and w_c is a design parameter that needs to be determined through tuning (Gao et al., 2001). In practical engineering situations, the parameter w_0 is the only parameter involved, which makes it easy to determine through trial and error. The function (fal) is important for the ESO system because of its characteristics of "big error, small gain; small error, big gain" when α_1 and $\alpha_2 < 1$. When α_1 and $\alpha_2 = 1$, this non-linear function turns into a linear one (Pu et al., 2015). The appropriate setting of the parameters β_1 , β_2 , and β_3 is crucial for achieving a dynamic response in ESO. By selecting suitable values of these parameters, the states \hat{x}_1 and \hat{x}_2 can track the output signal and its differential in the plant process, respectively. In addition, the extended state \hat{x}_3 is able to estimate the combined effect of uncertain models and system disturbances.

Considering the \bar{n} -DoF MM system (29) and the ESO (31), the estimated error system can be given as follows

$$\begin{cases} \dot{e}_1 = e_2 - \beta_1 e_1 \\ \dot{e}_2 = e_3 - \beta_2 f_1(e_1) \\ \dot{e}_3 = -h(t) - \beta_3 f_2(e_1) \end{cases} \quad (34)$$

where $e_2 \in \mathbb{R}^{\bar{n}}$ and $e_3 \in \mathbb{R}^{\bar{n}}$ are the observer's error for the states $x_2 \in \mathbb{R}^{\bar{n}}$ and $x_3 \in \mathbb{R}^{\bar{n}}$. According to analysis in Zhao et al. (2015), the convergence of the error system (34) is obtained using a self-stable region technique. Therefore, the

observed states \hat{x}_1 , \hat{x}_2 , and \hat{x}_3 converge to x_1 , x_2 , and x_3 , respectively.

Design of the ESO-based NFTSM

In this section, a composite NFTSM algorithm with ESO is introduced to control the MM system. The operating principle of the ESO is to estimate the system uncertainty and disturbance. The ESO requires the control input of the NFTSM and the system output. Then, it estimates state variables θ of the system, which includes the equivalent total disturbance observed. The output variable will be used by the NFTSM to modify the robust control law in real-time in order to reduce the effect of the disturbances.

According to Theorem 1, a robust control law based on ESO can be designed for tracking positions as

$$\begin{aligned} \bar{r} &= D^{-1}(x_1)(\bar{r}_{eq} + \bar{r}_b) \\ \bar{r}_{eq} &= - \left([e_2]^{\sigma_2 - I_{\bar{n}}} \right)^{-1} \sigma_2^{-1} k_2^{-1} \left(I_{\bar{n}} + k_1 \sigma_1 [e_1]^{\sigma_1 - I_{\bar{n}}} \right) e_2 \\ &\quad - \hat{x}_3 + \ddot{x}_d \\ \bar{r}_b &= -k_3 s - k_4 \text{sign}(s) \end{aligned} \quad (35)$$

The composite robust ESO-based NFTSM can be expressed as

$$\bar{r} = D^{-1}(x_1) \left(- \left([e_2]^{\sigma_2 - I_{\bar{n}}} \right)^{-1} \sigma_2^{-1} k_2^{-1} \left(I_{\bar{n}} + k_1 \sigma_1 [e_1]^{\sigma_1 - I_{\bar{n}}} \right) \cdot [e_1]^{\sigma_1 - I_{\bar{n}}} \cdot e_2 - \hat{x}_3 + \ddot{x}_d - k_3 s - k_4 \text{sign}(s) \right) \quad (36)$$

Assumption 2. Assuming that the derivative of \tilde{x}_3 is bounded, and there exists a constant $\tilde{\mu} > 0$, such as

$$\| \dot{\tilde{x}}_3(t) \| \leq \tilde{\mu} \quad \forall t \geq 0 \quad (37)$$

where $\tilde{x}_3 = x_3 - \hat{x}_3$ is the estimation error.

Theorem 2. Let the system (29) satisfies Assumption 2, applying the control law (36), the system state can converge to zero in finite time, if the gain satisfies $\| k_4 \| > \tilde{\mu}$.

Proof. According to equation (16), we can rewrite equation (22) as follows

$$\dot{s} = e_2 + k_1 \sigma_1 [e_1]^{\sigma_1 - I_{\bar{n}}} \cdot e_2 + k_2 \sigma_2 [e_2]^{\sigma_2 - I_{\bar{n}}} \cdot (x_3 + D(x_1)\bar{r} - \ddot{x}_d) \quad (38)$$

The time derivative of s becomes after substituting the control law (36)

$$\dot{s} = -k_2 \sigma_2 [e_2]^{\sigma_2 - I_{\bar{n}}} \cdot (-\tilde{x}_3 + k_3 s + k_4 \text{sign}(s)) \quad (39)$$

Performing the stability analysis based on the Lyapunov function $V_2 = 0.5s^T s$, its time derivative leads to

$$\dot{V}_2 = -s^T k_2 \sigma_2 [e_2]^{\sigma_2 - I_{\bar{n}}} \cdot (k_3 s + k_4 \text{sign}(s) - \tilde{x}_3) \quad (40)$$

According to Assumption 2, equation (40) can be rewritten as

$$\dot{V}_2 \leq -s^T k_2 \sigma_2 [e_2]^{\sigma_2 - I_{\bar{n}}} \cdot k_3 s - s^T k_2 \sigma_2 [e_2]^{\sigma_2 - I_{\bar{n}}} \text{sign}(s) (\bar{k}_4 - \tilde{\mu}) \leq 0 \quad (41)$$

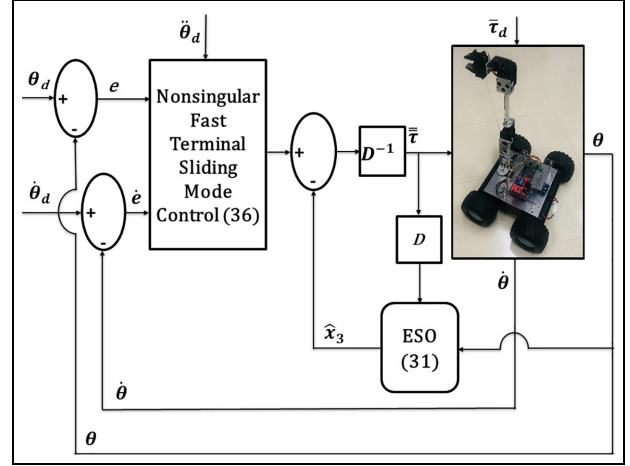


Figure 2. Structure of the ESO-based NFTSM controller for 5-DoF MM.

where $\bar{k}_4 = \lambda_{\min}(k_4)$ that represents the minimum eigenvalue of k_4 .

According to equation (41), it is verified from the above inequality with $\lambda_{\min}(k_4) > \tilde{\mu}$ that the system states converge to the $s = 0$ asymptotically. Therefore, the tracking errors can reach zero in finite time. The architecture of the ESO-based NFTSM controller for the 5-DoF MM is shown in Figure 2.

Remark 2. The estimated disturbance was obtained by the ESO and fed to the controller. However, estimation errors between the total disturbance value $f(x_1, x_2)$ and the estimated value \hat{x}_3 exist in the system. The proposed ESO-based NFTSM in this paper has the capability of rejecting the total disturbance. Besides, the MM closed-loop control system is converged to be stable if the parameter k_4 in the controller is tuned sufficiently large, which is derived from the Lyapunov principle. The following experimental results will validate this.

Experiments and discussion

Figure 3 shows the controller and hardware implementation structure as developed in the laboratory. A home-made MM robot called Mob-ETS is used in real-time practical implementation to verify the proposed control's satisfactory performance. The values of the RM physical parameters are given as $m_v = 2 \text{ kg}$, $r = 0.05 \text{ m}$, $2L = 0.27 \text{ m}$, and $I_v = 0.0122 \times 10^{-4} \text{ kg.m}^2$ and of the MP are given as $m_1 = 0.5 \text{ kg}$, $m_2 = 0.5 \text{ kg}$, $m_3 = 0.2 \text{ kg}$, $2L_1 = 0.16$, $2L_2 = 0.2$, $2L_3 = 0.12$, $I_1 = 2.666 \times 10^{-4} \text{ kg m}^2$, $I_2 = 1.16 \times 10^{-4} \text{ kg m}^2$ and $I_3 = 6.01 \times 10^{-4} \text{ kg m}^2$.

Simulink with Mathworks' Real-Time Workshop (RTW) is used to perform the ESO-based NFTSM on a 5-DoF MM in this experiment. The three joints of the RM, as well as the right and left wheels of the MP, are actuated by HN-GH12-2217Y DC-motors and Dynamixel motors (MX-64T), with encoder sensors (E4P-100-079-DH-T-B) utilized to calculate

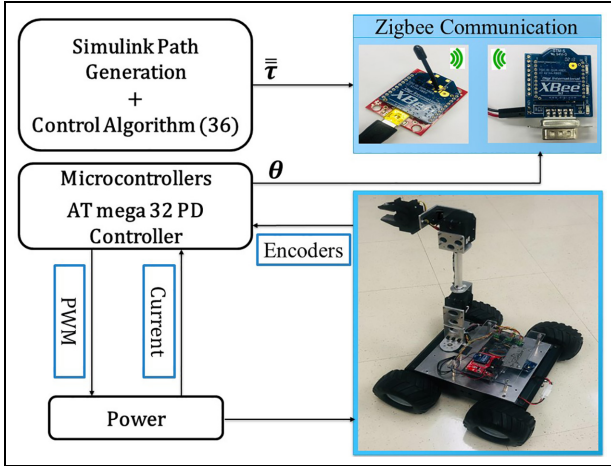


Figure 3. The structure of the experimental setup.

angular positions. Zigbee is used to communicate between the MATLAB/Simulink developed program and the MM.

For comparison purposes, the robust NFTSM described in Theorem 1 is applied to compare with the robustness of the proposed control approach in Theorem 2. The two control schemes, NFTSM and the proposed ESO-based NFTSM method, have been compared experimentally, for the end-effector being controlled to track the desired trajectory. The parameters of the NFTSM controller and the proposed controller are chosen with the same values as $\sigma_1 = 2$, $\sigma_2 = 5/3$, $k_1 = \text{diag}(0.001, \dots, 0.001) \in \mathbb{R}^{\bar{n}}$, $k_2 = \text{diag}(0.0018, \dots, 0.0018) \in \mathbb{R}^{\bar{n}}$, $k_3 = \text{diag}(36, \dots, 36) \in \mathbb{R}^{\bar{n}}$, and $k_4 = \text{diag}(215, \dots, 215) \in \mathbb{R}^{\bar{n}}$.

The empirical trial and error method is adopted in the experimental procedure to tune the control scheme parameters. First, the robust NFTSM is applied to control the MM, which assumes that the knowledge of the system uncertainty is known. Then, in the presence of the system uncertainty, the proposed ESO-based NFTSM's performance is validated for control system applications. The ESO has three types of parameters, based on the previously developed theory analysis of ESO, that is, a linear range δ , power terms $\alpha_{1,2}$, and gains β_i . The parameters of ESO are also tuned by the empirical trial and error method in the experimental part as $w_0 = 5$, $\delta = 0.01$, $\alpha_1 = 0.5$, and $\alpha_2 = 0.25$, where the bandwidth w_0 is used to tune the observer gains.

As a comparative result, the tracking performances of both controllers are represented in Figures 4–10. The trajectory tracking for the end-effector MM in the Cartesian space is shown in Figures 4 and 5. In both cases, the desired trajectory of the end-effector is a path in the XYZ space, which is selected with the starting point $P_s = [X_s, Y_s, Z_s, \phi_s]^T = [1.5, 0, 0.455, 0]^T$, the final point is $P_f = [X_f, Y_f, Z_f, \phi_f]^T = [5.5, 0, 0.42, 0]^T$. The inverse kinematics is used to obtain the desired trajectories in the joint space from the presented trajectory in Cartesian space of the end-effector.

Remark 3. In Theorem 1, the control law (21) is utilized to develop an NFTSM type of reaching law with term τ_{eq} (19) which can ensure the system's convergence in a fast-finite time. Whereas, the term τ_b (20) is adopted to enhance robustness against total disturbances. The stability of the closed-loop MM system was demonstrated in Theorem 2 using composite ESO-based NFTSM controller (40), based on Assumption 2 and assumes the upper bound of system

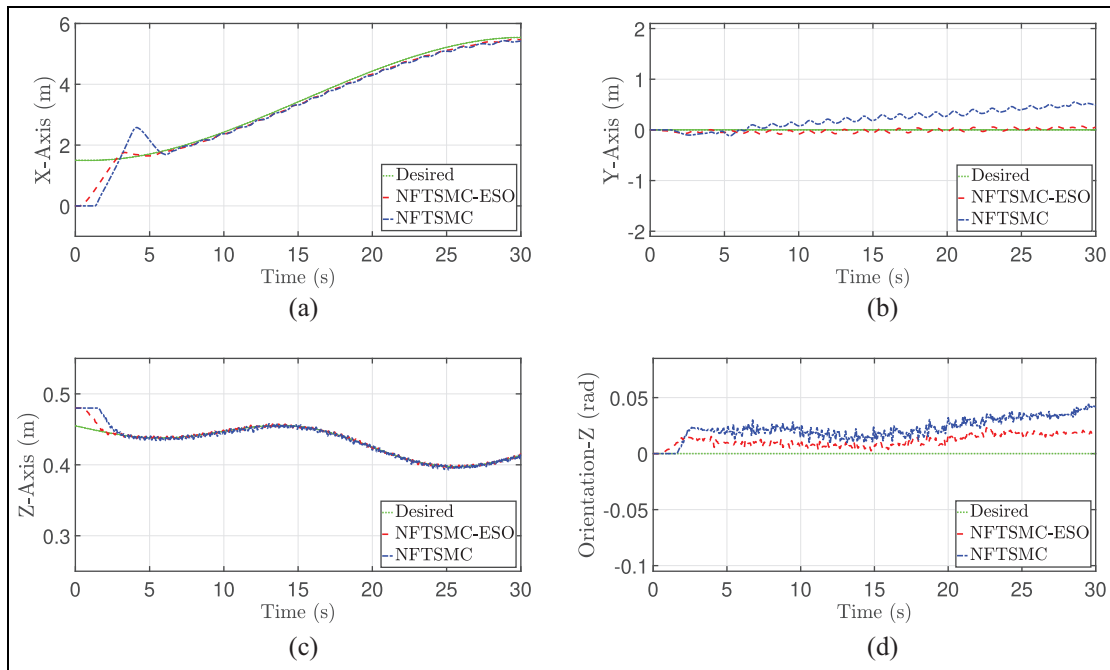


Figure 4. Trajectory tracking of the 5-DoF MM (X, Y, Z axes and orientation) in Cartesian space: (a) X-trajectory tracking, (b) Y-trajectory tracking, (c) Z-trajectory tracking, and (d) orientation trajectory tracking.

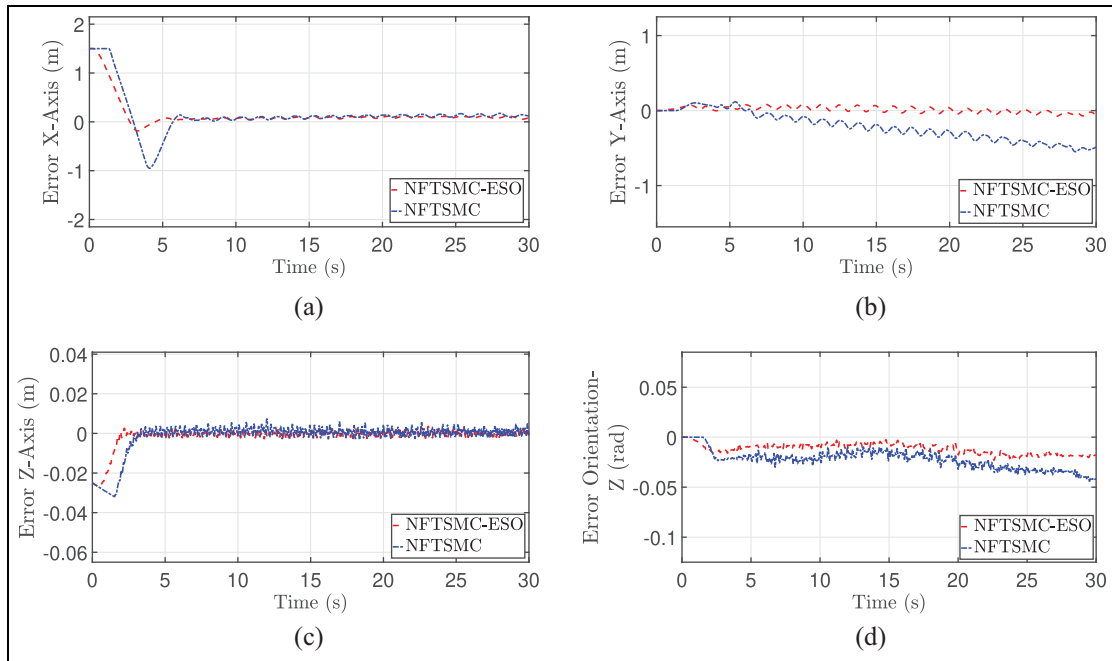


Figure 5. Tracking errors of the 5-DoF MM (X, Y, Z axes and orientation) in Cartesian space: (a) X-tracking error, (b) Y-tracking error, (c) Z-tracking error, and (d) orientation tracking error.

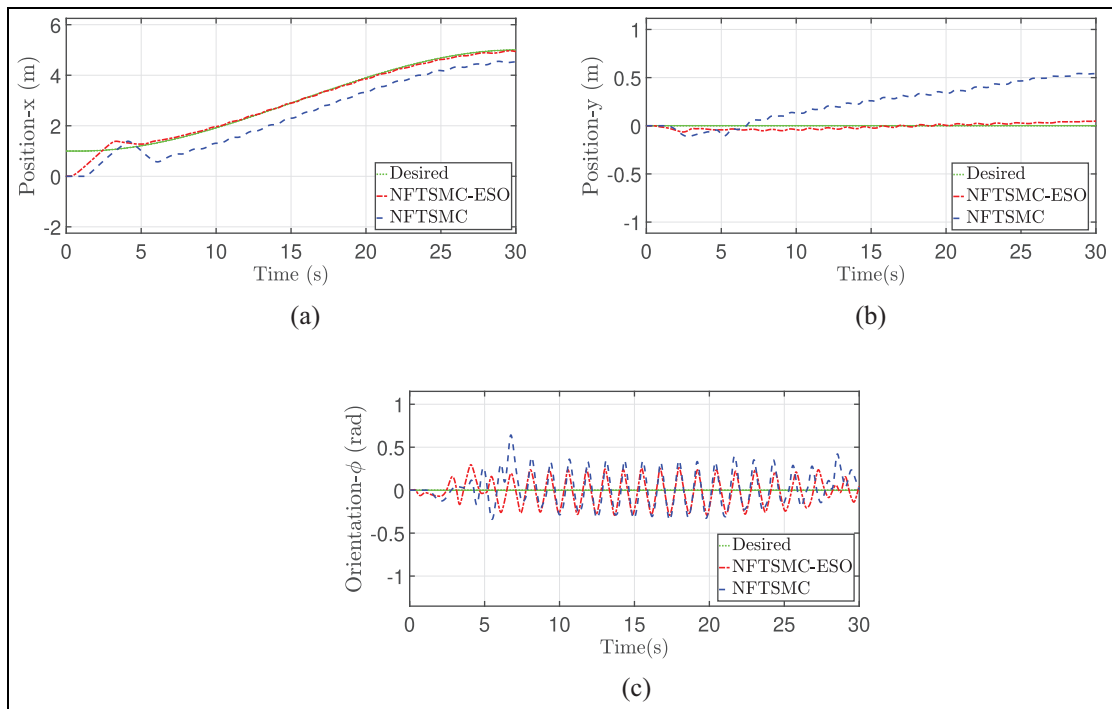


Figure 6. Trajectory tracking of the linear/angular position of the MP (x_v , y_v , and ϕ_v): (a) x_v -trajectory tracking (b) y_v -trajectory tracking, and (c) ϕ_v -trajectory tracking.

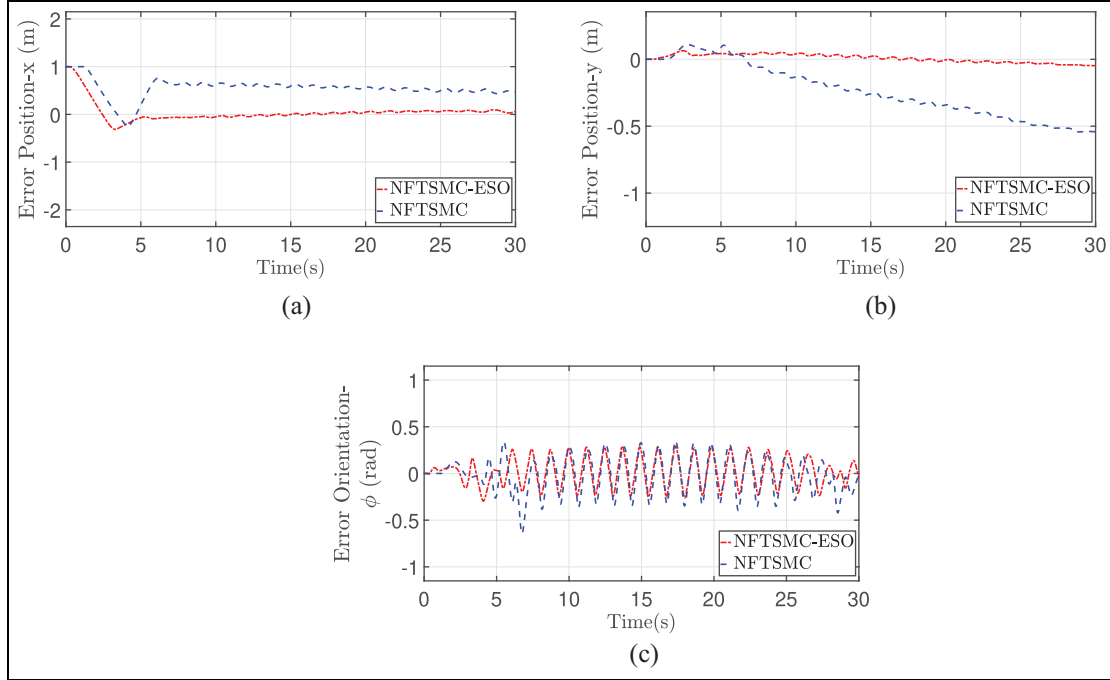


Figure 7. Tracking errors of the linear/angular position of the MP (x_v , y_v , and ϕ_v): (a) x_v -tracking error, (b) y_v -tracking error, and (c) ϕ -tracking error.

uncertainty. It is obvious that the proposed controller does not need exact knowledge of the system dynamics. The experimental findings have also demonstrated the excellent performance of the proposed method. Consequently, the contribution of this paper is confirmed.

Figure 4 shows the desired trajectory P_d of the end-effector P_e in Cartesian space as well as the actual position for the NFTSM with and without the ESO observer. Compared to NFTSM, the end-effector closely and consistently follows the desired trajectory when adding the observer. In addition, the convergence time with the NFTSM and ESO is less than 2.5 seconds, whereas it is more than 5 seconds with the NFTSM alone. Figure 5 shows the tracking errors for both methods. The tracking error amplitude is less than 0.1 mm which clearly reveals that the proposed ESO-based NFTSM scheme has better disturbance rejection and estimation with quick convergence of the system.

To present the robustness of the proposed ESO-based NFTSM scheme compared with the NFTSM, Figures 6 and 7 show the tracking position and tracking errors of the MP, respectively, with the maximum tracking error amplitude of 0.3 mm for x_v , y_v , and ϕ_v . As shown in these results, the responses of the ESO-based NFTSM scheme achieve superior robust performance compared with NFTSM. It can be verified that although the system uncertainties are unknown, the proposed control provides excellent experimental results and achieves good performances of trajectory tracking.

In Figure 8, the corresponding tracking of the three-dimensional (3D) figure end-effector and the two-dimensional (2D) figure MP positions are illustrated in Cartesian space. Figure 8 shows the comparison results of the (X ; Y ; Z) axes

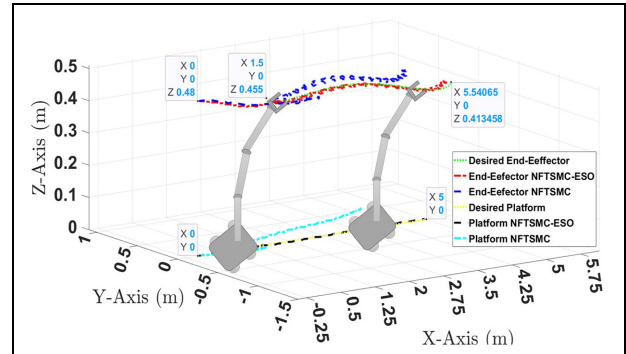


Figure 8. Tracking performance of the 5-DoF MM in Cartesian space (a) (X , Y , and Z) end-effector tracking in 3D and (b) (x_v , y_v) MP tracking in 2D.

and end-effector orientation and the (X ; Y) MP applying the NFTSM and ESO-based NFTSM controllers. The results indicate that the ESO-based NFTSM controller gives better results than the NFTSM controller.

In the joint-position trajectory tracking, Figure 9 shows the trajectory tracking of the MM in the joint space. Due to the obvious efficiency of the designed controller, the performed trajectory is very good. Figure 10 shows the tracking errors in the joint space for θ_R , θ_L , θ_1 , θ_2 , and θ_3 where the tracking errors are less than 0.5 rad. Thus, it is concluded that the ESO-based NFTSM has high performance, such as fast convergence, high tracking accuracy, singularity avoidance, and strong robustness against the total disturbances. The

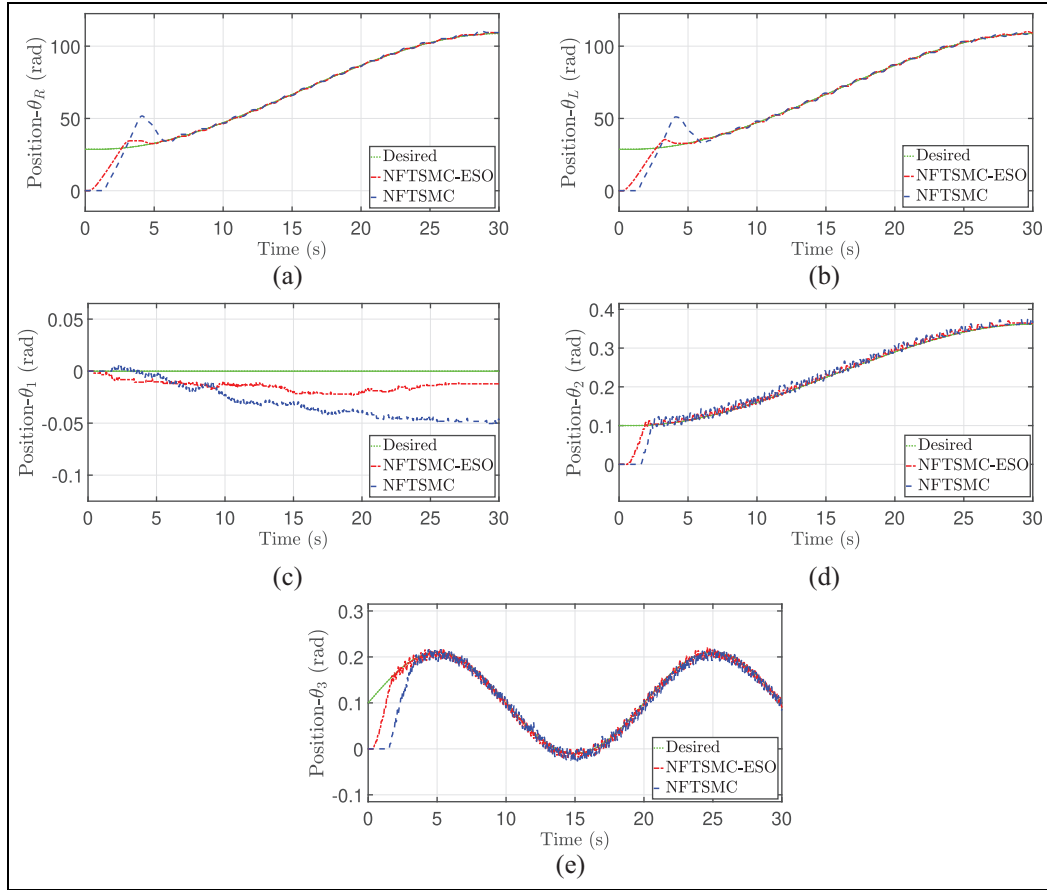


Figure 9. Trajectory tracking of the 5-DoF MM (θ_R , θ_L , θ_1 , θ_2 , and θ_3) in joint space: (a) position- θ_R trajectory tracking, (b) position- θ_L trajectory tracking, (c) position- θ_1 trajectory tracking, (d) position- θ_2 trajectory tracking, and (e) position- θ_3 trajectory tracking.

experimental results illustrate that the objective of the trajectory tracking control for the MM is successfully achieved with the composite ESO-based NFTSM controller in the presence of the system disturbances.

Figure 11 shows the applied control torques of the 5-DoF MM (τ_R ; τ_L ; τ_1 ; τ_2 ; τ_3). The experimental results depict the validity and efficiency of the proposed control and its ability to respond quickly to disturbances. Experimental tests were done by varying the controller gains by 30%. The obtained results are not depicted since a similar trajectory tracking performance and similar control efforts were obtained due to the accuracy of the ESO estimation.

Conclusion

In this paper, a robust ESO-based NFTSM control scheme was proposed for the MM system to overcome the problem of trajectory tracking. First, a dynamic model of the MM was given. The developed control law was then improved based on

the significant characteristics of the NFTSM principle, which can direct the system state to the origin within a prescribed finite time. However, with the NFTSM method, the complexity of the disturbances and uncertainties can be encountered, which often occurs in real-time applications. Finally, the composite ESO-based NFTSM for uncertainties and disturbances estimation has been introduced for more precise tracking. Moreover, it provides a faster convergence rate and good robustness compared to the NFTSM. Therefore, the ESO effectively estimates the total disturbances of the MM system. Based on NFTSM, the feedback control was designed to guarantee the closed-loop stability, and the proposed control was used to compensate for system uncertainties. The stability of the proposed control has been verified by the Lyapunov stability function. The experimental results clearly show that the ESO-based NFTSM controller achieved accurate tracking of the appropriate trajectory, with adequate tracking errors of the end-effector and joint positions, validating the effectiveness of the proposed approach for the 5-DoF MM in Cartesian space.

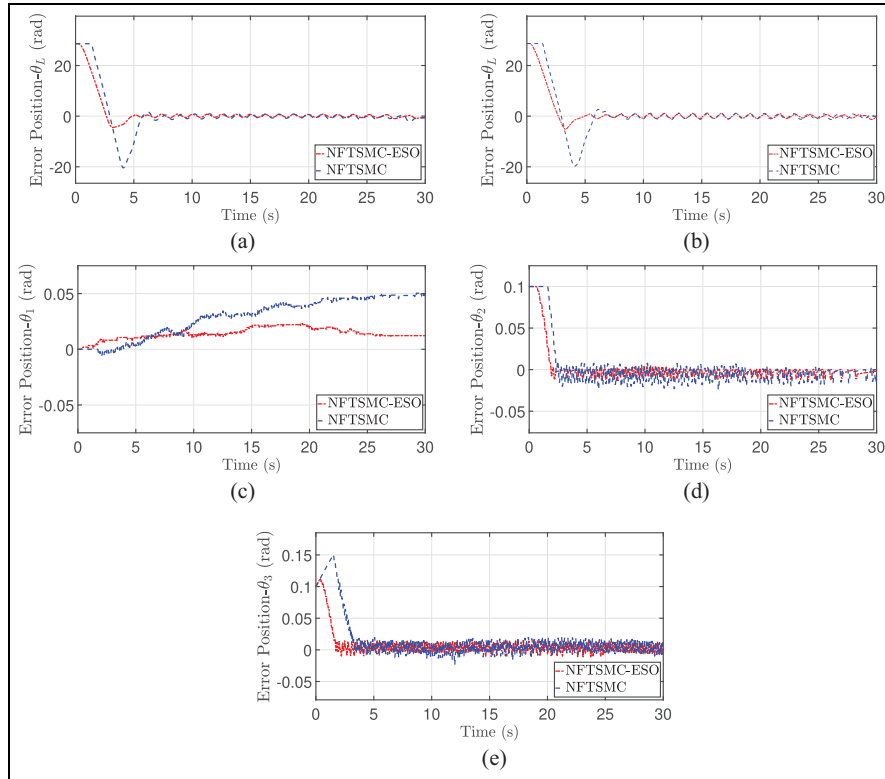


Figure 10. Tracking errors of the 5-DoF MM (θ_R , θ_L , θ_1 , θ_2 , and θ_3) in joint space: (a) position- θ_R tracking error, (b) position- θ_L tracking error, (c) position- θ_1 tracking error, (d) position- θ_2 tracking error, and (e) position- θ_3 tracking error.

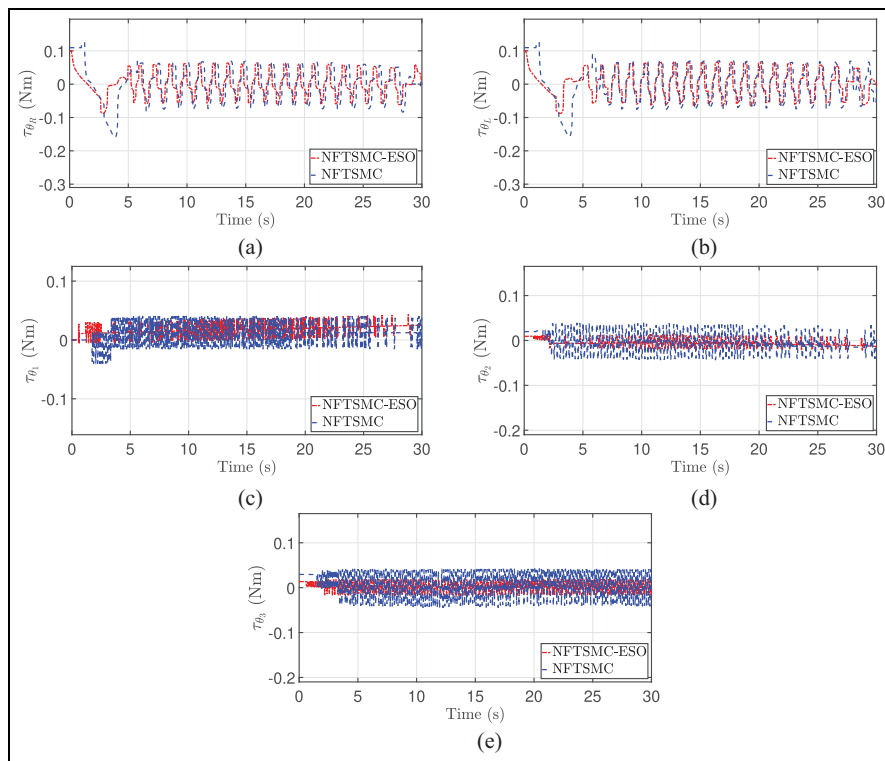


Figure 11. Control input signals for the 5-DoF MM (τ_R , τ_L , τ_1 , τ_2 , and τ_3): (a) input signal θ_R , (b) input signal θ_L , (c) input signal θ_1 , (d) input signal θ_2 , and (e) input signal θ_3 .


Declaration of conflicting interests

The author(s) declared no potential conflicts of interest with respect to the research, authorship, and/or publication of this article.

Funding

The author(s) received no financial support for the research, authorship, and/or publication of this article.

ORCID iD

Mhmed Algrnaodi  <https://orcid.org/0000-0002-0952-1625>

References

- Algrnaodi M, Saad M, Saad M, et al. (2021) Trajectory tracking for mobile manipulator based on nonlinear active disturbance rejection control. *International Journal of Modelling, Identification and Control* 37(2): 95–105.
- Andaluz V, Roberti F, Toibero JM, et al. (2012) Adaptive unified motion control of mobile manipulators. *Control Engineering Practice* 20(12): 1337–1352.
- Boukattaya M, Mezghani N and Damak T (2018) Adaptive nonsingular fast terminal sliding-mode control for the tracking problem of uncertain dynamical systems. *ISA Transactions* 77: 1–19.
- Brahmi A, Saad M, Gauthier G, et al. (2016) Adaptive backstepping control of mobile manipulator robot based on virtual decomposition approach. In: 2016 8th international conference on modelling, identification and control (ICMIC), Algiers, 15–17 November, pp. 707–712. New York: IEEE.
- Chen SY and Lin FJ (2010) Robust nonsingular terminal sliding-mode control for nonlinear magnetic bearing system. *IEEE Transactions on Control Systems Technology* 19(3): 636–643.
- Chung JH and Velinsky SA (1998) Modeling and control of a mobile manipulator. *Robotica* 16(6): 607–613.
- Dong W (2002) On trajectory and force tracking control of constrained mobile manipulators with parameter uncertainty. *Automatica* 38(9): 1475–1484.
- Fareh R, Brahmi A, Saad M, et al. (2017) Tracking control for nonholonomic mobile manipulator using decentralised control strategy. *International Journal of Modelling, Identification and Control* 28(1): 58–69.
- Fareh R, Khadraoui S, Abdallah MY, et al. (2021) Active disturbance rejection control for robotic systems: A review. *Mechatronics* 80: 102671.
- Feng Y, Yu X and Man Z (2002) Non-singular terminal sliding mode control of rigid manipulators. *Automatica* 38(12): 2159–2167.
- Gao Z, Hu S and Jiang F (2001) A novel motion control design approach based on active disturbance rejection. In: *Proceedings of the 40th IEEE conference on decision and control* (Cat. No. 01Ch37228), Orlando, FL, 4–7 December, pp. 4877–4882. New York: IEEE.
- Geng J, Sheng Y and Liu X (2014) Time-varying nonsingular terminal sliding mode control for robot manipulators. *Transactions of the Institute of Measurement and Control* 36(5): 604–617.
- Gu JJ and Wang JM (2018) Sliding mode control of the Orr–Sommerfeld equation cascaded by both the squire equation and ODE in the presence of boundary disturbances. *SIAM Journal on Control and Optimization* 56(2): 837–867.
- Gu JJ and Wang JM (2019) Sliding mode control for N-coupled reaction-diffusion PDEs with boundary input disturbances. *International Journal of Robust and Nonlinear Control* 29(5): 1437–1461.
- Han J (2009) From PID to active disturbance rejection control. *IEEE Transactions on Industrial Electronics* 56(3): 900–906.
- Hernandez JH, Cruz SS, López-Gutiérrez R, et al. (2020) Robust nonsingular fast terminal sliding-mode control for sit-to-stand task using a mobile lower limb exoskeleton. *Control Engineering Practice* 101: 104496.
- Huang Y and Xue W (2014) Active disturbance rejection control: Methodology and theoretical analysis. *ISA Transactions* 53(4): 963–976.
- Huang Y, Ma H, He Q, et al. (2022) Robust and compliance control for robotic knee prosthesis using admittance model and sliding-mode controller. *Transactions of the Institute of Measurement and Control* 44: 1088848.
- Jin M, Lee J, Chang PH, et al. (2009) Practical nonsingular terminal sliding-mode control of robot manipulators for high-accuracy tracking control. *IEEE Transactions on Industrial Electronics* 56(9): 3593–3601.
- Khan AH, Li S, Chen D, et al. (2020) Tracking control of redundant mobile manipulator: An RNN based metaheuristic approach. *Neurocomputing* 400: 272–284.
- Khawaf J, Zheng J, Lu R, et al. (2017) Robust tracking control of an IPMC actuator using nonsingular terminal sliding mode. *Smart Materials and Structures* 26(9): 095042.
- Labbadi M and Cherkaoui M (2020) Robust adaptive nonsingular fast terminal sliding-mode tracking control for an uncertain quadrotor UAV subjected to disturbances. *ISA Transactions* 99: 290–304.
- Li Z and Ge SS (2013) *Fundamentals in modeling and control of mobile manipulators* (Vol. 49). Boca Raton, FL: CRC Press.
- Li Z, Ge SS, Adams M, et al. (2008a) Robust adaptive control of uncertain force/motion constrained nonholonomic mobile manipulators. *Automatica* 44(3): 776–784.
- Li Z, Ge SS, Adams M, et al. (2008b) Adaptive robust output-feedback motion/force control of electrically driven nonholonomic mobile manipulators. *IEEE Transactions on Control Systems Technology* 16(6): 1308–1315.
- Li Z, Ge SS and Ming A (2007) Adaptive robust motion/force control of holonomic-constrained nonholonomic mobile manipulators. *IEEE Transactions on Systems, Man, and Cybernetics, Part B (Cybernetics)* 37(3): 607–616.
- Li Z, Ge SS and Wang Z (2008) Robust adaptive control of coordinated multiple mobile manipulators. *Mechatronics* 18(5–6): 239–250.
- Lu N, Ma L and Hua X (2022) Nonsingular fast terminal sliding mode control based on neural network with adaptive robust term for robotic manipulators with actuators. *Transactions of the Institute of Measurement and Control* 44: 3152.
- Madani T, Daachi B and Djouani K (2016a) Non-singular terminal sliding mode controller: Application to an actuated exoskeleton. *Mechatronics* 33: 136–145.
- Madani T, Daachi B and Djouani K (2016b) Modular-controller-design-based fast terminal sliding mode for articulated exoskeleton systems. *IEEE Transactions on Control Systems Technology* 25(3): 1133–1140.
- Mobayen S and Javadi S (2017) Disturbance observer and finite-time tracker design of disturbed third-order nonholonomic systems using terminal sliding mode. *Journal of Vibration and Control* 23(2): 181–189.
- Peng J, Yu J and Wang J (2014) Robust adaptive tracking control for nonholonomic mobile manipulator with uncertainties. *ISA Transactions* 53(4): 1035–1043.
- Pu Z, Yuan R, Yi J, et al. (2015) A class of adaptive extended state observers for nonlinear disturbed systems. *IEEE Transactions on Industrial Electronics* 62(9): 5858–5869.

- Rauf A, Zhao Z, Khan A, et al. (2022) Finite-time robust control of robotic manipulator with input deadzone and time-varying disturbance compensation. *Transactions of the Institute of Measurement and Control* 45: 6231.
- Savino HJ, Pimenta LC, Shah JA, et al. (2020) Pose consensus based on dual quaternion algebra with application to decentralized formation control of mobile manipulators. *Journal of the Franklin Institute* 357(1): 142–178.
- Song S, Tang C, Wang Z, et al. (2018) Active disturbance rejection controller design for stable walking of a compass-like biped. *Transactions of the Institute of Measurement and Control* 40(14): 4063–4077.
- Souzanchi KM, Arab A, Akbarzadeh TMR, et al. (2017) Robust impedance control of uncertain mobile manipulators using time-delay compensation. *IEEE Transactions on Control Systems Technology* 26(6): 1942–1953.
- Sun L and Liu Y (2020) Extended state observer augmented finite-time trajectory tracking control of uncertain mechanical systems. *Mechanical Systems and Signal Processing* 139: 106374.
- Taghavifar H and Rakheja S (2019) A novel terramechanics-based path-tracking control of terrain-based wheeled robot vehicle with matched-mismatched uncertainties. *IEEE Transactions on Vehicular Technology* 69(1): 67–77.
- Van M, Ge SS and Ren H (2016) Finite time fault tolerant control for robot manipulators using time delay estimation and continuous nonsingular fast terminal sliding mode control. *IEEE Transactions on Cybernetics* 47(7): 1681–1693.
- Walsh G, Tilbury D, Sastry S, et al. (1994) Stabilization of trajectories for systems with nonholonomic constraints. *IEEE Transactions on Automatic Control* 39(1): 216–222.
- Wang H, Li S, Lan Q, et al. (2017) Continuous terminal sliding mode control with extended state observer for PMSM speed regulation system. *Transactions of the Institute of Measurement and Control* 39(8): 1195–1204.
- Wu Y, Wang L, Zhang J, et al. (2019) Path following control of autonomous ground vehicle based on nonsingular terminal sliding mode and active disturbance rejection control. *IEEE Transactions on Vehicular Technology* 68(7): 6379–6390.
- Wu Y, Yu X and Man Z (1998) Terminal sliding mode control design for uncertain dynamic systems. *Systems & Control Letters* 34(5): 281–287.
- Xing HL, Jeon JH, Park KC, et al. (2011) Active disturbance rejection control for precise position tracking of ionic polymer–metal composite actuators. *IEEE/ASME Transactions on Mechatronics* 18(1): 86–95.
- Xu W, Junejo AK, Liu Y, et al. (2019) Improved continuous fast terminal sliding mode control with extended state observer for speed regulation of PMSM drive system. *IEEE Transactions on Vehicular Technology* 68(11): 10465–10476.
- Yamamoto Y and Yun X (1994) Modeling and compensation of the dynamic interaction of a mobile manipulator. In: *Proceedings of the 1994 IEEE international conference on robotics and automation*, San Diego, CA, 8–13 May, pp. 2187–2192. New York: IEEE.
- Yang J, Li S and Yu X (2012) Sliding-mode control for systems with mismatched uncertainties via a disturbance observer. *IEEE Transactions on Industrial Electronics* 60(1): 160–169.
- Yang J, Li S, Su J, et al. (2013) Continuous nonsingular terminal sliding mode control for systems with mismatched disturbances. *Automatica* 49(7): 2287–2291.
- Yang L and Yang J (2011) Nonsingular fast terminal sliding-mode control for nonlinear dynamical systems. *International Journal of Robust and Nonlinear Control* 21(16): 1865–1879.
- Yu Q and Chen IM (2002) A general approach to the dynamics of nonholonomic mobile manipulator systems. *Journal of Dynamics System and Measurements Control* 124(4): 512–521.
- Zhang Y, Chen Z and Sun M (2020) Trajectory tracking control for a quadrotor unmanned aerial vehicle based on dynamic surface active disturbance rejection control. *Transactions of the Institute of Measurement and Control* 42(12): 2198–2205.
- Zhao L, Cheng H and Wang T (2018) Sliding mode control for a two-joint coupling nonlinear system based on extended state observer. *ISA Transactions* 73: 130–140.
- Zhao L, Liu X and Wang T (2019) Trajectory tracking control for double-joint manipulator systems driven by pneumatic artificial muscles based on a nonlinear extended state observer. *Mechanical Systems and Signal Processing* 122: 307–320.
- Zhao L, Yang Y, Xia Y, et al. (2015) Active disturbance rejection position control for a magnetic rodless pneumatic cylinder. *IEEE Transactions on Industrial Electronics* 62(9): 5838–5846.
- Zhong G, Kobayashi Y, Hoshino Y, et al. (2013) System modeling and tracking control of mobile manipulator subjected to dynamic interaction and uncertainty. *Nonlinear Dynamics* 73(1): 167–182.